THE PHYSICS OF MECHANICAL ALLOYING IN A PLANETARY BALL MILL: MATHEMATICAL TREATMENT

M. ABDELLAOUI and E. GAFFET

CNRS-UPR A0423, "Far from Equilibrium Phase Transition Group", Institut Polytechnique de Sévenans,
90010 Belfort Cedex, France

Abstract—Based on a kinematic modeling of the planetary ball mill, the kinematic equations giving the velocity and the acceleration of a ball in a vial in a planetary ball mill are given. The kinetic energy transferred at the collision event, the shock frequency, and the injected shock power are also calculated. The confrontation of the calculated to some experimental results documented in the material literature, show that neither the shock energy nor the shock frequency separately taken into account, govern the end product but only the injected shock power is responsible for the ball milled end product.

1. INTRODUCTION

The results of the ball milling process are various. So, we can obtain the formation of amorphous phases by milling pure elements [1–3] or by milling elemental metal ribbons [4, 5] and the formation of intermetallics from pure elements [6, 7]. Also, mechanical alloying (MA) is a process used for producing powders having a fine microstructural scale [8] and/or a technique for alloying non-miscible materials [9]. Solid solution can also be considerably supersaturated compared to the thermodynamic equilibrium [10]. The process is also inherently flexible. As such, it is reasonable to expect it to grow in importance. However, there are considerable gaps in the fundamental knowledge base relative to MA, as there has been little attempt to analyse it in a manner that would establish predictive capabilities for it or at least determine the real physical parameter governing the phase transitions under this solicitation type. Thus, up to now, few attempts have been made to make a precise description of such a complex process.

Maurice and Courtney [11] try to give an approach defining the geometry and the basic mechanics of the powder-work piece interaction for several common devices used for MA, since these informations allow pertinent parameters of the process (e.g. impact velocity, powder material volume impacted, time between impacts, etc.) to be identified in terms of machine characteristics and process operating parameters. In the above mentioned work, three configurations were expected—a vertical mill such as the Szegvari attritor, the vibratory mill and the conventional horizontal ball mill. The numerical calculations show that the phase transitions are governed by only the injected shock energy.

Burgio *et al.* [12] attempt to correlate the milling operative conditions and the end product in a "Fritsch

Pulverisette P 5" ball mill. In the same mentioned work, the authors try to study the influence of the ball radius, the ball mass and the number of balls used on the end product. The shock frequency was assumed to scale with the relative velocity ω_r ($\omega_r = \omega_v - \Omega_p$ with ω_v and Ω_p respectively the vial and the disc rotation speeds).

Magini [13], using the difference between the potential energies before and after the collision event of a ball on a flat surface, calculates the kinetic shock energy released by the ball into the powders. The effect of the shock frequency is not taken into account at all.

Hachimoto *et al.* [14] calculate the shock energy consumption and the shock frequency during alloying using a vibrating ball mill. The authors conclude that the shock energy consumption is a function of a viscoelastic coefficient and increases with increasing this viscoelastic coefficient which has no physical meaning.

We have reported in our previous work [15], based on a mathematical treatment of the mechanical alloying process and experimental results on the ball-milled end product of the $Ni_{10}Zr_7$ compound, that neither the kinetic shock energy nor the shock frequency, separately taken into account, govern the end product. In other words, we proved that, at the stationary state, the end product depends only on the shock power, which is the product of the shock energy and the shock frequency.

The aim of this paper is to report on the details of such a mathematical treatment and the comparison of the experimental and the calculated results.

Since the kinetic shock energy consumption is not well defined until this moment, and to simplify the problem, the following assumptions are taken into

account to do the numerical calculations:

- the kinetic shock energy is released in totality into the powders,
- there is not relative motion between the ball and the vial wall prior to the departure point, i.e. the ball does not slip,
- after the flying time, the ball is newly attached to the wall without any elapsed time.

It is clear that the proposed collision model does not represent the real process but it is a useful simplification to determine the real physical parameter governing the far from equilibrium phase transitions induced by ball milling.

2. MATHEMATICAL TREATMENT OF THE PROCESS TAKING PLACE IN A PLANETARY BALL MILL

In the approximation of collision, Mc Kormick et al. [16] have done some improvement of the basic model of Burgio et al. [12] considering a "slip factor" that makes the trajectory of the flying ball rather different from the calculated one. A transparent top cover was used to allow the ball motion to be recorded using a high speed video camera [16]. The raw footage was edited and transferred to drawing software via an image analysis system [16]. Le Brun et al. [17] confirmed this by a videotape recording of this type of trajectory. The authors [16] state that a significant slip occurs between the ball and the wall of the vial. The relative ball/vial slip was characterized by defining a slip factor, f_s, where $f_s = 1 - \omega_b/\omega_r$ (ω_b is the relative angular velocity of the ball in contact with the vial wall) [16]. Taking into account this "slip factor" the authors [16] state that the value of the slip factor f_s has a larger effect on the departure frequency and that the shock frequency is directly determined by the product of the disc speed and $(1 - f_s)$. We agree with the assumption that the slip factor affects the shock frequency but we do not agree with the assumption which states that the shock frequency is the product of the disc rotation speed and $(1 - f_s)$ since we assume that shock frequency will be given by the inverse of one ball motion cycle duration.

Since, in the "Fritsch Pulverisette P7" planetary ball mill, the disc and the vial rotation speeds are coupled, the authors [16] are not able to study the effect of the kinetic shock energy, the shock frequency or the injected shock power separately taken into account. Thus, they state that the phase transitions or the kinetic reactions were governed only by the shock energy.

Our calculations were carried out for two planetary mills called G5 and G7. They exhibit respectively the same disc radius as the so called "Fritsch Pulverisette 5" and "Pulverisette 7". The aim of the construction of these two devices is the possibility of an independent variation of the disc and vial rotation speeds in order to study the shock energy, the shock frequency and the shock power effects.

In this section, the ball motion in the vial along one cycle is studied taking into account the above mentioned simplifying assumptions. Thus, the coordinates of the ball, when it is stuck to the inner vial surface and after leaving the inner vial surface (detachment event), are calculated. The equations proposed do not take into account the slip factor, really existing during the mechanical alloying process [16, 17], nevertheless they make a good approach to prove that neither the kinetic shock energy nor the shock frequency, taken into account separately, govern the phase transitions and that the end product depends only on the shock power.

The application of the fundamental dynamic principle gives the ball detachment condition which allows the calculation of the ball detachment position and the detachment velocity. These latter parameters (detachment position and detachment velocity) are used in order to calculate the motion of the ball from the detachment event until the collision one.

The ball collision velocity gives the kinetic energy released from the ball to the powders. The time needed between two collision events or two detachment events gives the shock frequency.

The modeling of the planetary ball mill is given in Fig. A1 and explained in paragraph A of the Appendix.

2.1. Absolute velocity and absolute acceleration of the ball before the detachment event

The adopted references (O, I, J, K) and (O$_1$, I, J, K) (Fig. A1) to do these calculations are Cartesian ones, with "O" the disc center and O$_1$ the vial center. The disc radius is taken as the distance between the disc center and the vial center such as $R = OO_1$. The ball is illustrated by the material "M" point. The vial rotation sense is the opposite of the disc one.

Based on Fig. A1, the "M" point position is defined as

$$OM = [R \cos(\theta) + r \cos(\alpha)]I$$
$$+ [R \sin(\theta) + r \sin(\alpha)]J. \quad (1)$$

The absolute velocity of the "M" point is given by the derivation of the OM vector expression given by equation (1) along the time. The final expression of the absolute velocity V_a and its amplitude are given in paragraph B of the Appendix as

$$V_a = [- R\Omega \sin(\theta) + rw \sin(\alpha)]I$$
$$+ [R\Omega \cos(\theta) \overset{\bullet}{-} rw \cos(\alpha)]J \quad (2)$$

$$\| V_a \|^2 = (R\Omega)^2 + (rw)^2 - 2Rr\Omega w \cos(\theta - \alpha). \quad (3)$$

The absolute acceleration γ_a of the point "M" obtained by the derivation of its absolute velocity V_a along the time, is given as follows

$$\gamma_a = \{- R\Omega^2 \cos(\theta) - rw^2 \cos(\alpha)\} I$$
$$+ \{- R\Omega^2 \sin(\theta) - rw^2 \sin(\alpha)\} J \quad (4)$$

or along the U_ρ and u_ρ vectors as

$$\gamma_a = -R\Omega^2 U_\rho - rw^2 u_\rho. \tag{5}$$

Its amplitude is given by

$$\|\gamma_a\|^2 = (R\Omega^2)^2 + (rw^2)^2$$
$$+ 2Rr\Omega^2 w^2 \cos(\theta - \alpha). \tag{6}$$

The expression (5) is illustrated in Fig. A2. It is the same expression as that given by Burgio et al. [12]. So, in this work, we try to give calculations of the kinetic shock energy, the shock frequency and the injected shock power taking into account the ball trajectory in the vial along one cycle.

2.2. Calculation of the detachment velocity and the detachment acceleration

Based on the fundamental dynamic principle, the resultant of the external forces acting on the ball is equal to the product of its mass by its acceleration. The physical forces applied to the ball are its weight (gravitational action) and the vial reaction. The ball weight is negligible as compared with the vial reaction. So, the resultant of the external forces is equal to the vial reaction, thus

$$F_1 (\text{vial reaction}) = m\gamma_a. \tag{7}$$

In a reference fixed to the ball, this latter is considered as fixed. So it will be submitted to two opposite forces: F_1, the vial reaction and F_2 such that the vectorial sum of F_1 and F_2 is equal to a null vector. Thus, the F_2 force is a centrifugal force such that $F_2 = -m\gamma_a$. So, the ball dynamic equilibrium is given as

$$-m\gamma_a + F_1 (\text{vial reaction}) = 0. \tag{8}$$

The resolution of equation (8) can be done easily when writing the absolute acceleration and the vial reaction as a function of the u_ρ and u_α vectors. The expression of the absolute acceleration is given in paragraph C of the Appendix as:

$$\gamma_a = [-R\Omega^2 \cos(\alpha - \theta) - rw^2]u_\rho$$
$$+ R\Omega^2 \sin(\alpha - \theta)u_\alpha. \tag{9}$$

By combining equations (8) and (9), and by writing the vial reaction F_1 as a sum of two components $F_{1\rho}$ and $F_{1\alpha}$, the following system is obtained

$$F_{1\rho} - m[-R\Omega^2 \cos(\alpha - \theta) - rw^2]u_\rho = 0 \tag{10a}$$

$$F_{1\alpha} - m[R\Omega^2 \sin(\alpha - \theta)]u_\alpha = 0 \tag{10b}$$

with $F_{1\rho}$ the normal vial reaction and $F_{1\alpha}$ the tangential vial reaction.

To have the detachment of the ball from the vial, we will have the cancellation of the normal vial reaction component $F_{1\rho}$ (component along the u_ρ vector). So, equation (10a) of the above mentioned system will be simplified as

$$\cos(\alpha - \theta) = -rw^2/R\Omega^2. \tag{11}$$

Thus, the amplitude of the absolute velocity and absolute acceleration at the detachment event, taking into account the detachment condition and the ball radius are the following:

$$\|V_a\|^2 = (R\Omega)^2 + (r - r_b)^2 w^2[1 + 2w/\Omega] \tag{12}$$

$$\|\gamma_a\|^2 = (R\Omega^2)^2 - [(r - r_b)w^2]^2. \tag{13}$$

2.3. Calculation of the collision point position

To obtain the time between detachment and collision events, a numerical solution using computer facilities is adopted. Figure A3 shows the ball motion from a detachment event up to a collision event, where (θ_d, α_d) and (θ_c, α_c) are the values of the disc and vial angular positions at the detachment and collision events respectively, V_d and V_c are the detachment and the collision velocities respectively, M_d and M_c are the ball positions at the detachment and the collision events respectively and $(u_{\rho d}, u_{\alpha d})$ and $(u_{\rho c}, u_{\alpha c})$ are the vectors defining the cylindrical referentials at the detachment and the collision events respectively. For the numerical calculations, to have an easy and clear geometrical formulation and further simplification of the parameter calculations, we assume that the θ_d value corresponding to the detachment event is equal to $\pi/2$. If we give another value to the θ_d angle, this will cause a change in the value of the α_d angle corresponding to the detachment event, but the calculation result will remain unchanged.

In the following calculations, the effective radius r^* which is equal to $(r - r_b)$ is taken into account instead of the vial radius "r". The detachment condition was given by equation (11). So, the detachment α_d angle value is given by the following expression

$$\cos\{(\pi/2) - \alpha_d\} = -w^2 r^*/\Omega^2 R \tag{14a}$$

which can be simplified as

$$\sin(\alpha_d) = -w^2 r^*/\Omega^2 R. \tag{14b}$$

When the effect of the gravitational force is neglected, the ball will follow a uniform linear motion with a constant velocity V_d and an initial position OM_d (Fig. A3). Its motion expression at a "t" instant after the detachment event is

$$OM = xI + yJ = V_d t + OM_d \tag{15}$$

which can be decomposed along the "X" and the "Y" axis, as [with $C = \sin(\alpha_d)$]

$$xI = V_{dx}t + OM_{dx}$$
$$= \{[-R\Omega + r^*wC]t + r^*(1 - C^2)^{0.5}\}I \tag{16a}$$

$$yJ = V_{dy}t + OM_{dy}$$
$$= \{-[r^*w(1 - C^2)^{0.5}]t + (R + r^*C)\}J. \tag{16b}$$

The details of such results are given in paragraph D of the Appendix.

At this same time "t", a "P" point of the vial has the following expression (in Fig. A3, the "M_c" point represents the "P" point at the collision event)

$$OP = [R \cos(\theta) + r^* \cos(\alpha)]\mathbf{I}$$

$$+ [R \sin(\theta) + r^* \sin(\alpha)]\mathbf{J}. \quad (17)$$

Writing: $OP_x = [R \cos(\theta) + r^* \cos(\alpha)]$ and $OP_y = [R \sin(\theta) + r^* \sin(\alpha)]$, with

$$\theta = \pi/2 + \Omega t \quad (18)$$

(at the "t" time equal to the 0, the θ angle is equal to $\pi/2$ which is the supposed first detachment angle).

The first collision event occurs when the following condition is fulfilled: $x = OP_x$ and $y = OP_y$, with x and y the ball coordinates after the detachment event and OP_x and OP_y represent the coordinates of the "P" point [the M_c point (Fig. A3)]. The numerical resolution consists to:

(1) increment of the time value by a time step interval "Δt" (μs),

(2) calculation of the θ angle value, given by equation (18),

(3) variation of the α angle value from 0 to -2π, by an increment of its value by a negative angle step interval $\Delta\alpha$ of $-0.01°$ (the $\Delta\alpha$ value is negative to have a vial rotation sense opposite to the disc one) and finally,

(4) calculation of the OP_x and OP_y values and x and y values. If the condition $x = OP_x$ and $y = OP_y$ is fulfilled, we have the first collision point coordinates values (x and y) along the "X" axis and the "Y" axis, the θ_c and α_c angular positions respectively of the disc and the ball in the vial, as well as the time "t" needed between the first detachment event and the first collision event.

2.4. Calculation of the kinetic energy by one hit

The kinetic energy "E_k" depends only on the ball detachment absolute velocity, since $\mathbf{V}_c = \mathbf{V}_d$. It is given by the following expression

$$E_k = 1/2m \, \|\mathbf{V}_c\|^2 = 1/2m \, \|\mathbf{V}_d\|^2. \quad (19)$$

As the angle between the collision velocity and the vial surface, at the collision event depends on the ball milling condition, the kinetic energy is decomposed into two components: the friction energy and the shock energy. To obtain a quantitative value of the friction energy and the shock energy, the collision velocity $\mathbf{V}_c$ will be decomposed into two components: a normal velocity $\mathbf{V}_{c\rho}$ and a tangential velocity $\mathbf{V}_{c\alpha}$ (Fig. A3). The normal velocity component is along the $\mathbf{u}_\rho$ vector (perpendicular to the vial surface) and induces the shock energy, the tangential velocity component is along the $\mathbf{u}_\alpha$ vector (parallel to the vial surface) and induces the friction energy. Thus, the friction kinetic energy "E_{fk}" is given as

$$E_{fk} = 1/2m \, \|\mathbf{V}_{c\alpha}\|^2 \quad (20a)$$

and the shock kinetic energy "E_{sk}" is given as

$$E_{sk} = 1/2m \, \|\mathbf{V}_{c\rho}\|^2. \quad (20b)$$

The expression of the normal velocity $\mathbf{V}_{c\rho}$ and the tangential velocity $\mathbf{V}_{c\alpha}$ are respectively given in paragraph E of the Appendix.

2.5. Calculation of the shock frequency

The shock frequency "f" is the number of collisions per second. Thus, the knowledge of the ball trajectory from the detachment event up to the collision event is required to calculate the shock frequency. The cycle period is decomposed into two periods T_1 and T_2 with T_1 the period of time needed by the ball to go from the detachment point up to the collision point and T_2 the period of time needed to have the first detachment event after the first collision one. The T_1 period value is calculated using the computer facilities. In other words, it is the "t" period such as the condition $x = OP_x$ and $y = OP_y$ that is fulfilled. Figure A4 shows the ball position to have the second detachment event, where (θ_c, α_c) and (θ_{d2}, α_{d2}) are the values of the disc and vial positions at the first collision and the second detachment events respectively, M_{d2} the ball position at the second detachment event and ($\mathbf{u}_{\rho d2}$, $\mathbf{u}_{\alpha d2}$) the vectors defining the cylindrical referential at the second detachment event. Based on Fig. A4, before the second detachment event, when the ball is stuck to the inner vial surface, it is submitted to the vial reaction $\mathbf{F}_{1\rho}$ such that

$$\mathbf{F}_{1\rho} + \gamma_{1\rho} = \mathbf{0} \quad (21a)$$

$$\mathbf{F}_{1\rho} - m [R\Omega^2 \cos(\beta) - r^*w^2]\mathbf{u}_\rho = \mathbf{0} \quad (21b)$$

with $\beta = -\pi + \lambda$ and $\lambda = \theta_{d2} + \eta$ and $\eta = -2\pi - \alpha_{d2}$.

To have the second detachment of the ball from the inner vial surface, we will have the cancellation of the normal vial reaction component $\mathbf{F}_{1\rho}$, as it was assumed in equation (10a). Thus, to have the second detachment event the following condition will be fulfilled

$$-m [- (r^*w^2)$$

$$+ R\Omega^2 \cos(-\pi + (\theta_{d2} - 2\pi - \alpha_{d2}))]\mathbf{u}_\rho = \mathbf{0}.$$

This latter can be simplified as

$$r^*w^2/R\Omega^2 = \cos(-3\pi + \theta_{d2} - \alpha_{d2}). \quad (21c)$$

The θ_{d2} and α_{d2} angles correspond, respectively, to the positions of the disc and the ball in the vial at the second detachment event (Fig. A4). They are given by the following equations

$$\theta_{d2} = \theta_c + \Omega T_2 \quad \text{and} \quad \alpha_{d2} = \alpha_c - wT_2 \quad (22)$$

with θ_c and α_c, the values of the angular positions respectively of the disc and the ball in the vial at the first collision event and T_2 the time period needed, after the first collision event, to reach the second detachment event. The values of θ_c and α_c angular positions are given by the computer calculations and correspond to the satisfaction of the $x = OP_x$ and $y = OP_y$ conditions. To calculate the T_2 period, we will replace the θ_{d2} and α_{d2} angles by their above mentioned expressions (22), in equation (21c).

After replacement, we have

$$T_2 = [3\pi - (\theta_c - \alpha_c)$$
$$+ \arccos(r^* w^2 / R\Omega^2)]/(\Omega + w). \quad (23)$$

As the cycle period "T" is the sum of the two period components T_1 and T_2, the shock frequency value is given by the inverse of the cycle period and is given by the following expression

$$f = \frac{1}{T_1 + T_2}. \quad (24)$$

This shock frequency corresponds to one ball. So, when operating with a given number of balls, the shock frequency is equal to the product of one ball frequency with the balls number corrected by a factor $\leqslant 1$. The fact is studied above by Burgio *et al.* [11].

Based on Fig. A4, it is easy to see that the decomposition of the absolute acceleration into its two components and the absolute intensities of these latter are the same as those reported in Fig. A2 and the disc position is the same as that reported in Fig. A3 but shifted by an angle value equal to Ω $(T_1 + T_2)$. Thus, we conclude that we have a real periodicity of the ball motion in the vial.

2.6. Calculation of the shock power

The power released by the ball to the powders is the product of the frequency with the kinetic energy. It is given by the following expression

$$P = \frac{1}{T} \int_0^T dE_k = f E_k. \quad (25)$$

The cumulated kinetic energy released from the ball to the powders during a ball milling duration "BMD", is given by the product of the shock power [equation (25)] by the ball milling duration value.

3. NUMERICAL CALCULATIONS RESULTS

Our calculations are carried out for two planetary ball mills called G5 and G7. The so called G5 and G7 planetary ball mills exhibit respectively the same disc radius as the so called Fritsch "Pulverisette 5" and "Pulverisette 7". The aims of the construction of these two devices are first, the possibility of variation of the disc and vial rotation speeds independently and second, the study of the disc radius effect on the kinetic energy, the shock frequency and the shock power. Furthermore, an ultrasonic tachometer control during the milling process allows a true control of the effective vials and disc rotations speeds.

The disc radius corresponding to the so called G5 and G7 planetary ball mills are respectively equal to 132×10^{-3} and 75×10^{-3} m. The vial radius is equal to 21×10^{-3} m. The ball radius and the ball mass are respectively equal to 7.5×10^{-3} m and 14 g. Five balls are used in order to calculate the shock energy, the shock frequency and the shock power.

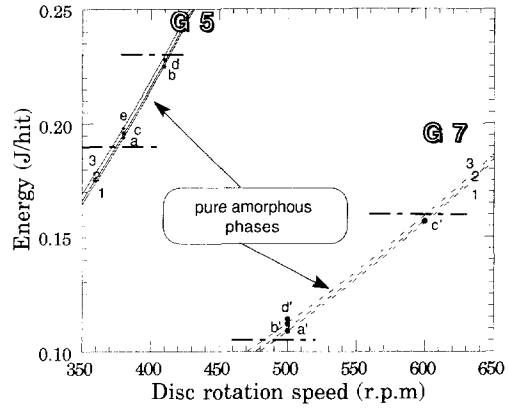Figures 1, 2 and 3 (solid line: G5 mill and dashed line: G7 mill) give the kinetic energy released from one

Fig. 1. Kinetic energy by one hit as a function of the disc and the vial rotation speeds corresponding to the G5 (—) and the G7 (– – –) planetary ball mills. The vial rotation speed values are referred by the numbers 1, 2 and 3 written near each corresponding curve: 1 = 150, 2 = 250 and 3 = 350 rpm. The kinetic energies corresponding to the experimental ball milling conditions illustrated in Fig. 4 by the data points a, b, c, d and e for the G5 device and a′, b′, c′ and d′ for the G7 device, leading to the same pure amorphous phases formation are reported [15].

ball to the powders in one hit, the shock frequency and the shock power as a function of the disc and the vial rotation speeds [15].

Based on these above mentioned figures, the kinetic energy and the shock power increase as a function of the disc and vial rotation speeds. The shock frequency drastically decreases and then increases almost linearly as the disc rotation speed increases. For the so called G5 planetary ball mill, the maximum kinetic energy can reach 0.9 J/hit (0.3 J/hit for the G7 device), for a disc and vial rotation speeds respectively equal to
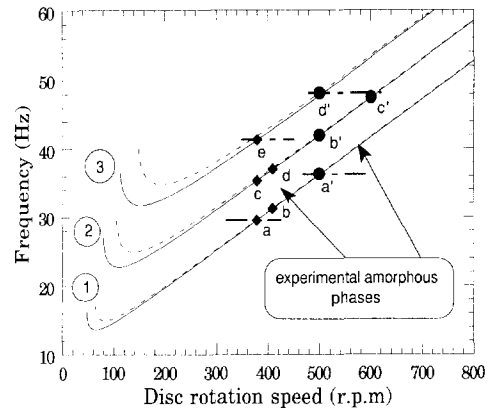

Fig. 2. Shock frequency as a function of the disc and vial rotation speeds for the G5 (—) and G7 (– – –) planetary ball mills. The vial rotation speed values (in rpm) are referred by the numbers 1, 2, and 3 written near each corresponding curve: 1 = 150, 2 = 250 and 3 = 150 rpm. The shock frequencies corresponding to the experimental ball milling conditions illustrated in Fig. 4 by the data points a, b, c, d and e for the G5 device and a′, b′, c′ and d′ for the G7 device, leading to pure amorphous phases formation are reported [15].
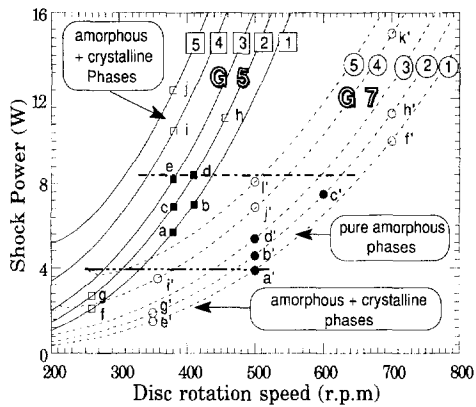
Fig. 3. Shock power as a function of the disc and vial rotation speeds for the G5 (—) and G7 (– – –) planetary ball mills. The vial rotation speed values (in rpm) are referred by the numbers 1, 2, 3, 4 and 5 written near each corresponding curve: $1 = 150$, $2 = 250$, $3 = 350$, $4 = 500$ and $5 = 600$ rpm. The shock powers corresponding to the experimental ball milling conditions illustrated in Fig. 4 by the data points a, b, c, d and e for the G5 device and a′, b′, c′ and d′ for the G7 device, leading to the same pure amorphous phases formation as well as the shock power values corresponding to the experimental ball milling conditions, illustrated in Fig 4 by the data points f, g, h, i and j for the G5 device and e′, f′, g′, h′, i′, j′, k′ and l′ for the G7 device, leading to the formation of a mixture of crystalline and amorphous phases are reported [15]

Fig. 4. Superimposition of the end-product structure corresponding to the ball milling of the $Ni_{10}Zr_7$ compound at room temperature by means of the G5 and G7 machine. On the left Y-axis, the Ω_{G7} rotation speeds are reported, on the right Y-axis, the Ω_{G5} values are noted. The filled symbols correspond to pure amorphous phases, whereas the half-filled symbols correspond to mixture of crystalline and amorphous phases. The dashed areas correspond to the two amorphous domains [15].

800 and 800 rpm. The shock frequency and shock power can respectively reach 90.7 Hz (92.4 Hz for the G7 device) and 80.2 W (28 W for the G7 device) for a disc and vial rotation speeds equal respectively to 800 and 800 rpm.

4. APPLICATION TO THE $Ni_{10}Zr_7$ COMPOUND

Gaffet *et al.* [18] have used the G5 and G7 ball-milling machines to study the effect of the ball milling conditions on the end product in the $Ni_{10}Zr_7$ compound. In this work [18], 10 g of molten spun ribbon pieces of mean composition $Ni_{58.8}Zr_{41.2}$ (in atomic percent), corresponding to the $Ni_{10}Zr_7$ intermetallic compound are introduced into a cylindrical tempered steel container of capacity 45 ml. This procedure is carried out in a glove-box filled with purified argon. Each container is loaded with five steel balls of 1.5 cm dia and 14 g mass. The containers are sealed in the glove-box with a Teflon O-ring and the milling proceeds in a stationary argon atmosphere. *The ball milling duration corresponding to the stationary state is 48 h (the use of a ball milling duration greater than 48 h does not change the end product result. The initial state (prealloyed elemental component material) does not effect the end product).* The structures of the as-spun ribbons have been checked by X-ray diffraction (XRD) patterns and have been confirmed to correspond purely to the $Ni_{10}Zr_7$ intermetallic compound. For the ball milled samples, a numerical method "ABFfit program" was used in order to analyze the XRD patterns and to obtain the position and the
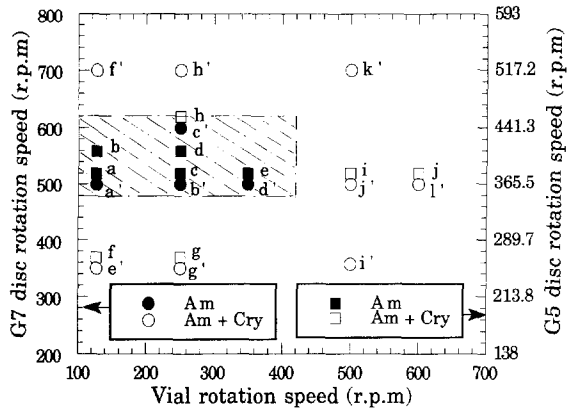
full width at half height of the various peaks. *The crystalline phases taken into account are those which correspond to the equilibrium phases in the Ni–Zr phase diagram.* The same authors [18] report on the experimental ball milling conditions leading to the formation of pure amorphous phases and the formation of a mixture of amorphous and crystalline phases. Figure 4 [15] illustrates the [18] data and shows a dynamic phase diagram mapped into two regions: a pure amorphous phase region (filled symbols) and mixture of crystalline and amorphous phases region (half-filled symbols). The hatched areas correspond to the two amorphous domains.

Eckert *et al.* [19] elaborate amorphous powders by mechanical alloying from Ni–Zr crystalline elemental powders. The mechanical alloying was performed in a conventional planetary ball mill (Fritsch "Pulverisette 5"). The ball milling intensities used are 3, 5 and 7. The authors [19] show that for ball milling intensity 5 a pure amorphous phase is formed from about 30 to 83 at.% Ni. The ball milling duration required to achieve the amorphization process was 60 h. For ball milling intensity 7, for the same ball milling duration (60 h), the authors report on the formation of an intermetallic phase form $x = 66$ to 75 at.% Ni. For ball milling intensity 3, the amorphization is not achieved even at extended ball milling duration.

Based on our mathematical treatment of the process taking place in the planetary ball mill, the calculated shock energies corresponding to the experimental ball milling conditions leading to the amorphous phases formation [18] are reported in Fig. 1 [15]. The calculated shock energies leading to the amorphous phase formation for the G5 device (lozenge symbol) range from about 194×10^{-3} to about 227×10^{-3} J/hit. For the G7 ball mill (circle symbol), the calculated

shock energies leading to the same amorphous phases as the G5 one, range from about 109×10^{-3} to about 157×10^{-3} J/hit.

As shown in Fig. 1 [15], there is no overlapping between the two energy domains corresponding to the same amorphous phases formation when using the G5 and G7 devices. The calculated shock frequencies corresponding to the experimental ball milling conditions leading to the amorphous phases formation are reported in Fig. 2 [15]. As concluded above for the shock energy, there is no perfect overlapping between the two frequency domains corresponding to the same amorphous phases formation when using the two devices. The calculated shock powers corresponding to the experimental ball milling conditions leading to the amorphous phase formation are reported in Fig. 3 [15]. Based on this figure, there is a perfect overlapping between the shock power domains leading to the same amorphous phases induced when using the G5 (square symbols) and G7 (circle symbols) devices. Moreover, when considering Fig. 3 [15] the calculated shock powers corresponding to the experimental ball milling conditions leading to the formation of a mixture of crystalline and amorphous phases [15] (f, g, h, i and j points for the G5 device and e′, f′, g′, h′, i′ and k′ points for the G7 device), we see that the power values corresponding to these experimental data points lie outside the shock power domain corresponding to pure amorphous phase formation (bounded by the two horizontal chain lines). Thus, we conclude that neither the shock energy nor the shock frequency, separately taken into account, govern the end product but only the injected shock power is responsible for the ball milled end product.

Based on the experimental results [18] and the calculated results, the amorphous phase formation is allowed for the shock power ranging from 4 to 8.2 W. The ball milling duration, corresponding to the stationary state, used to obtain the amorphous phases either by the G5 or the G7 planetary ball mill is 48 h [18] and all the ball milling durations greater than or equal to 48 h do not change the ball milled end product obtained for 48 h. Figure 3 [15] illustrates the dynamically end product phase diagram which is mapped into three regions as a function of the shock power; a first corresponding to the formation of a mixture of amorphous and crystalline phases reported for the low power values, a second corresponding to the formation of pure amorphous phases reported for the medium power values and finally a third corresponding to the formation of a mixture of amorphous and crystalline phases reported for high power values. The crystalline phases obtained even for low or high injected shock powers correspond to the $Ni_{10}Zr_7$ intermetallic compound.

We assume that if the shock power is lower than a minimum value, mechanical alloying induces, after a long ball milling duration, only a refinement of the powder grain size and an increase of the defect quantity until reaching a steady state which is not able to be destabilized into another structural state, whereas, if the shock power is greater than a minimum power value, mechanical alloying induces a refinement of the powder grain size and an increase of the defect quantity at a rate able to induce, even in the earlier stages of mechanical alloying, a mixture of structurally transformed phase and initial phase. In the latter case, the steady state can result, depending on the value of the shock power, in a mixture of structurally transformed phase and initial phase or in a homogeneous structurally transformed phase. The steady state is reached when elastic energy storage in the powder become impossible.

We assume that for the low shock power values, the increase of the free energy of the crystalline powders, due to the increase of the defect concentration induced by plastic deformation is not high enough to promote the formation of only a pure amorphous phase and the input crystalline phases are able to remain crystalline at even a such shock power. For the medium shock power level, the defect concentration, $G_c + \Delta G_d > G_a$, where G_c is the free energy of the crystalline phase, ΔG_d is the increase in the free energy due to the defects introduced by MA and G_a is the free energy of the amorphous phase. Thus, only a pure amorphous phase is able to be formed. This fact is reported by Brimhall et al. [20] and Schwarz et al. [21]. For the high shock power level, we have, as like the low power level, formation of a mixture of crystalline and amorphous phases.

Eckert et al. [19] assume that the temperature during mechanical alloying is a very important parameter of the process. They conclude that partial crystallization can occur during mechanical alloying at high milling intensities. Thus the crystallization can not simply be caused by the milling but must be an effect of excess heating during mechanical alloying. Based on the procedure proposed by Schwarz et al. [21], they estimate the peak temperature reached within the powder particles during milling. They obtained $\Delta T = 130, 247$ and $407°C$ for intensities 3, 5 and 7 respectively. Since an isothermal anneal of the amorphous powders at 400°C for only 5 min is sufficient to produce partially crystallized materials with a similar X-ray diffraction pattern to that obtained for the $Ni_{70}Zr_{30}$ powder milled for 60 h at intensity 7, the authors [19] conclude that the actual temperature of the individual particles during mechanical alloying can in fact be rather high—at least high enough to cause the crystallization of the formed amorphous particles. Miller et al. [22], using microsecond time-resolved radiometry, observed temperature increases of the order of 400–500°C upon impacting NaCl crystals. Davies et al. [23] report on the ball milling of the brittle elements Si and Ge. Based on the procedure proposed by Schwarz et al. [21], they estimated the temperature rise in the ball milled Si and Ge to respectively $\Delta T = 6.57$ and 10.1 K.

Table 1. Documented [24] and calculated values (*: this work) of the kinetic energy, the shock frequency and the shock power for the different ball mills

| | Attritor | Vibratory mills | | Planetary ball mills | | |
		Pulv. O	SPEX	Pulv. P5	G7	G5
Velocity of balls (m/s)	0–0.8	0.14–0.24	<3.9	2.5–4	0.24–6.58 *	0.28–11.24 *
Kinetic energy (10^{-3} J/hit)	<10	3–30	<120	10–400	0.4–303.2 *	0.53–884 *
Shock frequency (Hz)	>1000	15–50	200	~100	5.0–92.4 *	4.5–90.7 *
Power (W/g/ball)	<0.001	0.005–0.14	<0.24	0.01–0.8	0–0.56 *	0–1.604 *

In a first analysis, we see that there is no agreement between the above-reported estimated temperature rises. All the same, it is important to note that these temperature rises will induce many structural phase transitions. Thus, we think that the crystalline phase obtained for high shock power values (Fig. 3) can be the result of a partial crystallization of the formed amorphous due to the excess of heating.

The assumption of a total release of the kinetic shock energy may translate the levels of the three domains of the dynamical phase diagram shown in Fig. 3 but it does not change its shape and, whatever the shock energy consumption percent, the amorphization proceeds above a minimum power input and below a certain maximum power input.

More discussions of the phase transition mechanisms induced by mechanical alloying are recently reported in our previous work [15].

Chen et al. [24] report some results documented on the materials literature concerning the kinetic energy, the shock frequency and the shock power for three most common devices: the Attritor ball mill, the planetary ball mill (Fritsch "Pulverisette P5") and the vibratory grinder (e.g. SPEX shaker mill). Table 1 gives the documented values [24] and the calculated values (for the G5 and G7 planetary ball mill) of the kinetic energy, the shock frequency and the shock power.

Based on Table 1, the G5 shock power domain covers all the other devices shock power domains. More, it was reported by Martin et al. [25], that the ball milling power input domain covers some typical mechanical straining or irradiating power input domains. Thus we assume that the G5 planetary ball mill is able to induce the same phase transitions which can be induced by all the other devices.

5. CONCLUSIONS

Based on a mathematical treatment of the process taking place in a planetary ball mill, taking into account many simplifying assumptions mentioned in the beginning, the kinematic equations giving the velocity and the acceleration of a ball in vial in a planetary ball mill are given. The kinetic energy transferred at the collision event, the shock frequency and the shock power are also calculated. The con-

frontation of the calculation results to experimental results, show that, at the stationary state, neither the shock energy nor the shock frequency, separately taken into account, govern the end product but only the injected shock power is responsible for the ball milled end product.

Based on our calculation results and Gaffet et al. [18] experimental results, a dynamic end product phase diagram is mapped into three regions as a function of the shock power, a first corresponding to the formation of a mixture of amorphous and crystalline ($Ni_{10}Zr_7$ intermetallic compound) phases reported for the low power level, a second corresponding to the formation of pure amorphous phases reported for the medium power level and finally a third corresponding to the formation of a mixture of amorphous and crystalline ($Ni_{10}Zr_7$ intermetallic compound) phases.

The reported equations will be improved by taking into account the slip factor of the ball/wall at the detachment event and the elapsed time at the collision event. Moreover, more searches of the mechanical alloying at the local level are needed to have the really released shock energy and the free energy excess in connection with the injected shock power.

REFERENCES

1. E. Gaffet, Mater. Sci. Engng. A136, 161 (1991).
   For recent conferences: Int. Symp. Mech. Alloying Kyoto, Japan (edited by P. H. Shingu). Trans. Tech. Publications (1991). Solid-St. Amorphizing Transformations (organized by R. B. Schwarz and W. L. Johnson), Los Alamos, U.S.A. (1987). Symp. Int. Amorphization by Solid-St. Reaction (organized by A. R. Yavari, E. Gaffet, J. M. Legresy and F. Bordeaux) Grenoble, France (1990). ASM Int. Conf. (organized by F. H. Froes and J. J. DeBarbadillo) Myrtle Beach, S.C., U.S.A. (1990). European Workshop on Ordering and Disordering (organized by A. R. Yavari and P. Desré), Grenoble, France (1991).
2. E. Gaffet and M. Harmelin, J. less-common Metals. 157, 201 (1990).
3. M. Sherif El-Eskandarany, Kiyoshi Aoki, Haruko Itoh and Kenji Suzuki, J. less-common Metals. 169, 235 (1991).

4. F. Bordeaux and A. R. Yavari, *J. Appl. Phys.* **67**, 2385 (1990).
5. A. Calka, A. P. Pogany, R. A. Shanks and H. Engelman, *Mater. Sci. Engng* **A128**, 107 (1990).
6. T. J. Tianen and R. B. Schwarz, *J. less-common metals.* **140**, 99 (1988).
7. M. S. Kim and C. C. Koch, *J. Appl. Phys.* **62**, 3450 (1987).
8. C. Suryanarayana and F. H. Froes, *Nanostruct. Mater.* **1**, 191 (1992).
9. E. Gaffet, C. Louison, M. Harmelin and F. Faudot, *Mater. Sci. Engng.* **A134**, 1380 (1991).
10. A. Abdellaoui, T. Barradi and E. Gaffet, *J. Alloys. Comp.* **198**, 155 (1993).
11. D. R. Maurice and T. H. Courtney, *Metall. Trans. A*, **21A**, 289 (1990).
12. N. Burgio, A. Iasonna, M. Magini, S. Martelli and F. Padella, *Il Nuovo Cimento.* **13D**, 459.
13. M. Magini, *Mater. Sci. For.* **88–90**, 121 (1992).
14. H. Hachimoto and R. Watanabe, *Mater. Trans. JIM*, **31**, 219 (1990).
15. M. Abdellaoui and E. Gaffet, *J. All. Comp.* **209**, 351 (1994).
16. P. G. Mc Kormick, H. Huang, M. P. Dallimore, J. Ding and J. Pan, *Proc. 2nd Int. Conf. Struct. Applic. Mech. Alloying* (edited by J. J. de Barbadillo, F. H. Froes and R. Schwarz), pp. 45–50. ASM, Vancouver (1993).
17. P. Le Brun, L. Froyen and L. Delaey, *Mater. Sci. Engng.* **A161**, 75 (1993).
18. E. Gaffet and L. Yousfi, *Mater. Sci. Forum* **88–90**, 51 (1992).
19. J. Eckert, L. Schultz, E. Hellstern and K. Urbain, *J. Appl. Phys.* **64**, 3224 (1988).
20. J. L. Brimhall, H. E. Kissinger and L. A. Charlot, *Radiat. Eff.* **77**, 237 (1983).
21. R. B. Schwarz and C. C. Koch, *Appl. Phys. Lett.* **49**, 146 (1986).
22. P. J. Miller, C. S. Coffey and V. F. Devost, *J. Appl. Phys.* **59**, 913 (1986).
23. R. M. Davies and C. C. Koch, *Scripta metall.* **21**, 305 (1987).
24. Y. Chen, R. Le Hazif and G. Martin, *Solid-St. Phen.* **23 & 24**, 271 (1992).
25. G. Martin and E. Gaffet, Colloque de Physique, Colloque C4, Supplément au No. 14, Tome 51, 71 (1990).

APPENDIX

(A) References and "M" Point Position Expression

Fig. A1 shows the ball position "M" at a "t" event.
R: disc radius (m), r: vial radius (m), r_b: ball radius (m), m: ball mass (kg), "M", a material point representing the ball position in the vial.

$\theta = \Omega t$, the disc rotation angle with $\mathbf{\Omega} = \Omega \mathbf{K}$, the angular disc rotation speed.

$\alpha = -wt$, the vial rotation angle with $\mathbf{w} = -w\mathbf{K}$ the angular vial rotation speed.

$\mathbf{U}_\rho \| \mathbf{R}$ and $\mathbf{U}_\theta \perp \mathbf{U}_\rho, \mathbf{u}_\rho \| \mathbf{r}$ and $\mathbf{u}_z \perp \mathbf{u}_\rho$.

Based on Fig. A1, $\mathbf{OM} = \mathbf{OO_1} + \mathbf{O_1 M} = R\mathbf{U}_\rho + r\mathbf{u}_\rho$.
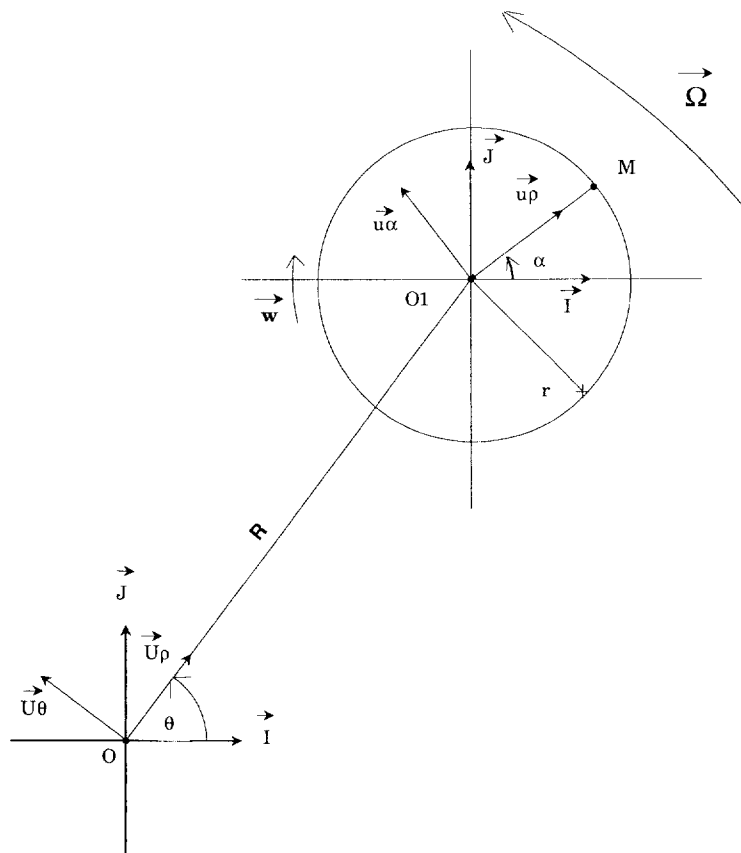

Fig. A1. Geometry of the disc and one vial seen from the top. The various vectors and angles are explained in the text [15].

(B) Calculation of the Absolute Velocity

The absolute velocity $\mathbf{V}_a$ of the point "M" is given as following

$$\mathbf{V}_a = \frac{dR}{dt} \mathbf{U}_\rho + R \frac{d\mathbf{U}_\rho}{dt} + \frac{dr}{dt} \mathbf{u}_\rho + r \frac{d\mathbf{u}_\rho}{dt}. \quad (B1)$$

Thus, as the two radii R and r, respectively of the disc and the vial, are constant in time, the expression of the absolute velocity is simplified to

$$\mathbf{V}_a = R \frac{d\mathbf{U}_\rho}{dt} + r \frac{d\mathbf{u}_\rho}{dt} \quad (B2)$$

or as, $\mathbf{U}_\rho = \cos(\theta)\mathbf{I} + \sin(\theta)\mathbf{J}$ and $\mathbf{u}_\rho = \cos(\alpha)\mathbf{I} + \sin(\alpha)\mathbf{J}$, the absolute velocity is given by $\mathbf{V}_a = R \ (d\theta/dt) [-\sin(\theta)\mathbf{I} + \cos(\theta)\mathbf{J}] + r \ (d\alpha/dt) \ [-\sin(\alpha)\mathbf{I} + \cos(\alpha)\mathbf{J}]$ and as, $d\theta/dt = \Omega$ and $d\alpha/dt = -w$, the expression of the absolute velocity is given by

$$\mathbf{V}_a = R\Omega[-\sin(\theta)\mathbf{I} + \cos(\theta)\mathbf{J}]$$
$$- r\omega [-\sin(\alpha)\mathbf{I} + \cos(\alpha)\mathbf{J}] \quad (B3)$$

and as, $\mathbf{U}_\theta = -\sin(\theta)\mathbf{I} + \cos(\theta)\mathbf{J}$ and $\mathbf{u}_\alpha = -\sin(\alpha)\mathbf{I} + \cos(\alpha)\mathbf{J}$,

$$\mathbf{V}_a = R\Omega\mathbf{U}_\theta - rw\mathbf{u}_\alpha = \mathbf{\Omega} \wedge R\mathbf{U}_\rho + \mathbf{w} \wedge r\mathbf{u}_\rho. \quad (B4)$$

The final expression of the absolute velocity $\mathbf{V}_a$ in the Cartesian reference $(O, \mathbf{I}, \mathbf{J}, \mathbf{K})$ and its amplitude are respectively given as

$$\mathbf{V}_a = [-R\Omega \sin(\theta) + rw \sin(\alpha)]\mathbf{I}$$
$$+ [R\Omega \cos(\theta) - rw \cos(\alpha)]\mathbf{J}. \quad (B5)$$

$$\| \mathbf{V}_a \|^2 = (R\Omega)^2 + (rw)^2 - 2Rr\Omega w \cos(\theta - \alpha). \quad (B6)$$

(C) Decomposition of the Absolute Acceleration

Based on equation (5), the absolute acceleration γ_a can be decomposed into two components γ_1 and γ_2 such as $\gamma_1 = -R\Omega^2 \mathbf{U}_\rho$ and $\gamma_2 = -rw^2\mathbf{u}_\rho$. To be attached to the vial, the ball will be submitted to a centrifugal force along the $\mathbf{u}_\rho$ vector. To have the detachment of the ball from the vial, the above mentioned centrifugal force will be cancelled and becomes central just after that. To formulate this detachment condition, we must decompose the absolute acceleration into two components the first along the $\mathbf{u}_\rho$ vector and the second along the $\mathbf{u}_\alpha$ vector. From Fig. A2, the component γ_1 can be decomposed into two components $\gamma_{1\rho}$ and $\gamma_{1\alpha}$ such as

$$\gamma_{1\rho} = -R\Omega^2 \cos(\alpha - \theta)\mathbf{u}_\rho$$

and

$$\gamma_{1\alpha} = R\Omega^2 \sin(\alpha - \theta)\mathbf{u}_\alpha.$$

Thus, the absolute acceleration can be formulated, taking into account the new formulation of the γ_1 component, as following

$$\gamma_a = [-R\Omega^2 \cos(\alpha - \theta) - rw^2]\mathbf{u}_\rho$$
$$+ R\Omega^2 \sin(\alpha - \theta)\mathbf{u}_\alpha. \quad (C1)$$

(D) Cartesian Expressions of the Detachment Velocity and Detachment Position

The expression of the absolute velocity is given by equation (B5). Taking into account that, at the first detachment event, $\theta_d = \pi/2$ and $\sin(\alpha_d) = -w^2r^*/\Omega^2R$ (Fig. A3), the expression of the detachment velocity $\mathbf{V}_d$ is

$$\mathbf{V}_d = [-R\Omega + r^*w(-w^2r^*/\Omega^2R)]\mathbf{I} - r^*w \cos(\alpha_d)\mathbf{J}. \quad (D1)$$

$$\beta = -\pi - (\alpha - \theta)$$
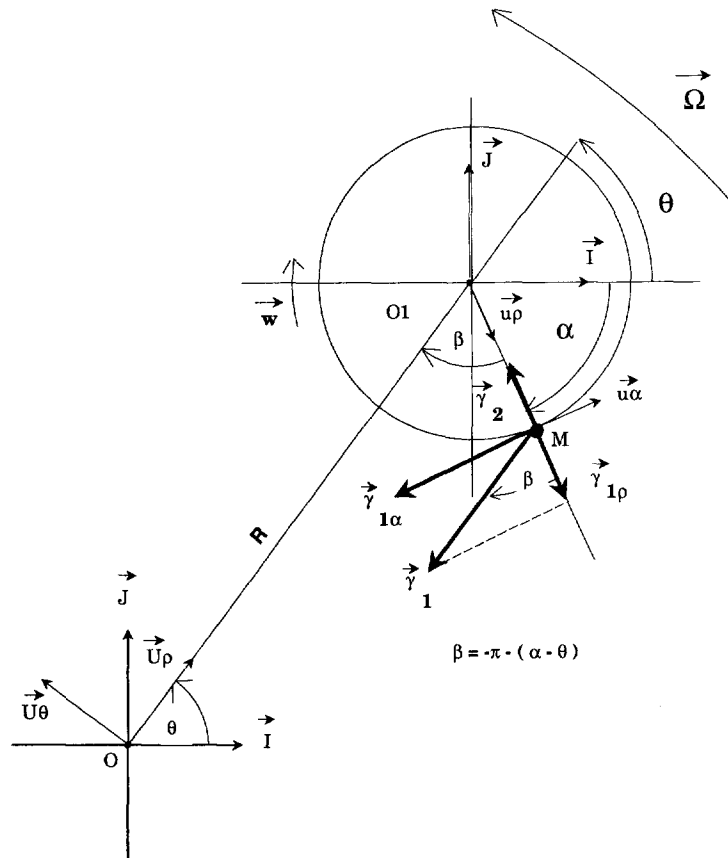
Fig. A2. Decomposition of the ball absolute acceleration.

Fig. A3. Absolute velocity and ball position at the detachment and collision events. The various vectors are explained in the text [15].

Fig. A4. Ball position and absolute acceleration at the second detachment event.

The detachment velocity can be decomposed into two components $\mathbf{V}_{dx}$ along the "X" axis and $\mathbf{V}_{dy}$ along the "Y" axis such as

$$\mathbf{V}_{dx} = [-R\Omega + r^*wC]\mathbf{I}$$

and

$$\mathbf{V}_{dy} = -[r^*w(1 - C^2)^{0.5}]\mathbf{J}. \qquad \text{(D2)}$$

Above the detachment event, $\mathbf{OM} = R[\cos(\theta)\mathbf{I} + \sin(\theta)\mathbf{J}] + r^*[\cos(\alpha)\mathbf{I} + \sin(\alpha)\mathbf{J}]$. Taking into account the same above mentioned detachment conditions, the vectorial "M" point position $\mathbf{OM}_d$, will be as following

$$\mathbf{OM}_d = r^*\cos(\alpha_d)\mathbf{I} + [R + r^*\sin(\alpha_d)]\mathbf{J}. \qquad \text{(D3)}$$

This vectorial position can be decomposed into two components $\mathbf{OM}_{dx}$ along the "X" axis and $\mathbf{OM}_{dy}$ along the "Y" axis such as

$$\mathbf{OM}_{dx} = r^*(1 - C^2)^{0.5}\mathbf{I}$$

and

$$\mathbf{OM}_{dy} = (R + r^*C)\mathbf{J} \qquad \text{(D4)}$$

with $C = \sin(\alpha_d)$.

(E) Calculation of the Normal and Tangential Velocities at the Collision Event

As $\mathbf{I} = \cos(\alpha)\mathbf{u}_\rho - \sin(\alpha)\mathbf{u}_\alpha$ and $\mathbf{J} = \sin(\alpha)\mathbf{u}_\rho + \cos(\alpha)\mathbf{u}_\alpha$, the collision velocity given by equation (D1), will be

$$\mathbf{V}_c = \{(-R\Omega + r^*wC)\cos(\alpha)$$
$$- r^*w(1 - C^2)^{0.5}\sin(\alpha)\}\mathbf{u}_\rho$$
$$- \{(-R\Omega + r^*wC)\sin(\alpha)$$
$$+ r^*w(1 - C^2)^{0.5}\cos(\alpha)\}\mathbf{u}_\alpha. \qquad \text{(E1)}$$

This latter can be easily decomposed into two components $\mathbf{V}_{c\rho}$, the normal velocity and $\mathbf{V}_{c\alpha}$, the tangential velocity (Fig. A3) such as

$$\mathbf{V}_{c\rho} = \{(-R\Omega + r^*wC)\cos(\alpha)$$
$$- r^*w(1 - C^2)^{0.5}\sin(\alpha)\}\mathbf{u}_\rho \qquad \text{(E2)}$$

$$\mathbf{V}_{c\alpha} = -\{(-R\Omega + r^*wC)\sin(\alpha)$$
$$+ r^*w(1 - C^2)^{0.5}\cos(\alpha)\}\mathbf{u}_\alpha. \qquad \text{(E3)}$$